Steel and Composite Structures, *Vol. 25, No. 3 (2017) 347-360*
DOI: https://doi.org/10.12989/scs.2017.25.3.347

Vibration and mode shape analysis of sandwich panel with MWCNTs FG-reinforcement core

Vahid Tahouneh*

Young Researchers and Elite Club, Islamshahr Branch, Islamic Azad University, Islamshahr, Iran

(*Received April 08, 2017, Revised June 26, 2017, Accepted July 11, 2017*)

Abstract. The goal of this study is to fill this apparent gap in the area about vibration analysis of multiwalled carbon nanotubes (MWCNTs) curved panels by providing 3-D vibration analysis results for functionally graded multiwalled carbon nanotubes (FG-MWCNTs) sandwich structure with power-law distribution of nanotube. The effective material properties of the FG-MWCNT structures are estimated using a modified Halpin-Tsai equation. Modified Halpin-Tsai equation was used to evaluate the Young's modulus of MWCNT/epoxy composite samples by the incorporation of an orientation as well as an exponential shape factor in the equation. The exponential shape factor modifies the Halpin-Tsai equation from expressing a straight line to a nonlinear one in the MWCNTs wt% range considered. Also, the mass density and Poisson's ratio of the MWCNT/phenolic composite are considered based on the rule of mixtures. Parametric studies are carried out to highlight the influence of MWCNT volume fraction in the thickness, different types of CNT distribution, boundary conditions and geometrical parameters on vibrational behavior of FG-MWCNT thick curved panels. Because of using two-dimensional generalized differential quadrature method, the present approach makes possible vibration analysis of cylindrical panels with two opposite axial edges simply supported and arbitrary boundary conditions including Free, Simply supported and Clamped at the curved edges. For an overall comprehension on 3-D vibration analysis of sandwich panel, some mode shape contour plots are reported in this research work.

Keywords: FG-MWCNT structures; vibration; thick laminated structures; three-dimensional theory of elasticity; Halpin-Tsai equation; mode shape analysis

1. Introduction

Functionally graded cylindrical panels, as important structural components, have been widely used in different engineering branches such as mechanical, energy and aerospace engineering. However, in comparison with the isotropic and conventional laminated cylindrical panels, the literature on the free vibration analysis of FG cylindrical panels is relatively scarce. In addition, in the most of the existing researches in this regards, single layer FG cylindrical panels have been widely analyzed. In the following, some of these research works are briefly reviewed.

Due to the mismatch of stiffness properties between the face sheets and the core, sandwich plates and panels are susceptible to face sheet/core debonding, which is a major problem in sandwich construction, especially under impact loading (Abrate 1998). Various material profiles through the functionally graded plate and panel thickness can be illustrated by using parameter power-law distribution. In fact, by considering power-law distribution, it is possible to study the influence of different kinds of material profiles. Recently, Viola and Tornabene (2009) used three-parameter power-law distribution to study the dynamic behavior of functionally graded parabolic panels of revolution. Though there are research works reported on general sandwich structures, very little work has been done to consider the vibration behavior and static response of FGM structures (Anderson 2003, Kashtalyan and Menshykova 2009, Barka *et al.* 2016, Chen *et al.* 2017, Tornabene *et al.* 2016a, b). Fantuzzi et al. (2016) used Non-Uniform Rational B-Spline (NURBS) curves to describe arbitrary shapes with holes and discontinuities. By means of above-mentioned method, they have analyzed free vibration of arbitrarily shaped FG carbon nanotube-reinforced plates. Brischetto *et al*. (2015) studied free vibration of simply supported Single- and Double-Walled Carbon Nanotubes (SWCNTs and DWCNTs). A continuum approach (based on an elastic three-dimensional shell model) was used for natural frequency investigation of SWCNTs and DWCNTs. SWCNTs were defined as isotropic cylinders with an equivalent thickness and Young modulus. DWCNTs were defined as two concentric isotropic cylinders (with an equivalent thickness and Young modulus). Li *et al.* (2008) studied free vibrations of FG sandwich rectangular plates with simply supported and clamped edges. Zenkour (2005a,b) presented a two-dimensional solution to study the bending, buckling and free vibration of simply supported FG ceramic-metal sandwich plates. Kamarian *et al.* (2013) studied free vibration of FGSW rectangular plates with simply supported edges and rested on elastic foundations using differential quadratic method. The natural frequencies of FGM circular cylindrical shells were investigated by Loy *et al*. (1999), which was later extended to cylindrical shells under various end supporting conditions (Pradhan *et al.* 2000). Patel *et al.* (2005) carried out the vibration analysis

*Corresponding author, Ph.D.,
E-mail: vahid.tahouneh@ut.ac.ir

ISSN: 1229-9367 (Print), 1598-6233 (Online)

of functionally graded shell using a higher-order theory. Pradyumna *et al.* (2008) studied the free vibrations analysis of functionally graded curved panels via a higher-order finite element formulation. Free vibration and dynamic instability of FGM cylindrical panels under combined static and periodic axial forces were studied by using a proposed semi-analytical approach (Yang and Shen 2003). Elastic response analysis of simply supported FGM cylindrical shell under low-velocity impact was presented by Gang *et al.* (1999). Vibrations and wave propagation velocity in a functionally graded hollow cylinder were studied by Shakeri *et al*. (2006). They assumed that the shell to be in plane strain condition and subjected to an axisymmetric dynamic loading. The free vibration of simply supported, fluid-filled cylindrically orthotropic functionally graded cylindrical shells with arbitrary thickness was investigated by Chen *et al.* (2004). Recently, Tornabene (2009) used four-parameter power-law distribution to study the dynamic behavior of moderately thick functionally graded conical and cylindrical shells. In his study, the two-constituent functionally graded isotropic shell was consisted of ceramic and metal, and the generalized differential quadrature method was used to discretize the governing equations. Static and free vibration analyses of continuously graded fiber-reinforced cylindrical shells via generalized power-law distribution were presented by Sobhani Aragh and Yas (2010a). Also, these authors (2010b) investigated three-dimensional free vibration of functionally graded fiber orientation and volume fraction of cylindrical panels. Paliwal *et al.* (1995, 1996) have investigated the free vibration of whole buried cylindrical shells with simply supported ends in contact with Winkler and Pasternak foundations using direct solution to the governing classical shell theory equations of motion. Bouguenina *et al*. (2015) studied FG plates with variable thickness subjected to thermal buckling. Wu and Liu (2016) developed a state space differential reproducing kernel (DRK) method in order to study 3D analysis of FG circular plates. Park *et al.* (2016) used modified couple stress based third-order shear deformation theory for dynamic analysis of sigmoid functionally graded materials (S-FGM) plates. Yang *et al.* (1998) have investigated the behavior of whole buried pipelines subjected to sinusoidal seismic waves by the finite element method. Cai *et al.* (2000) have investigated free vibration of a cylindrical panel resting on Kerr foundation. Kerr model can be reduced to either a Pasternak model or a Winkler one by selecting certain values of foundation parameters. Gunawan *et al.* (2006) examined the free vibrations of cylindrical shells partially buried in elastic foundations based on the finite element method. The shells were discretized into cylindrical finite elements, and the distribution of the foundation in the circumferential direction, was defined by the expansion of Fourier series.

Tornabene and Ceruti (2013) studied a mixed static and dynamic optimization of four-parameter functionally graded material (FGM) doubly curved shells and panels. The functionally graded shell consists of ceramic and metal, and the volume fraction profile of each lamina varies through the thickness of the shell according to a generalized power-law distribution. Free vibration and stability of functionally graded shallow shells according to a 2-D higher order deformation theory were investigated by Matsunaga (2008). Civalek (2005) investigated the nonlinear dynamic response of doubly curved shallow shells resting on Winkler–Pasternak elastic foundations using the harmonic differential quadrature (HDQ) and finite differences (FD) methods. Hong and Lee (2015) presented a spectral element model for a modified FGM axial bar model wherein non-uniform lateral contraction in the thickness direction was taken into account. Marin and Marinescu (1998), studied thermoelasticity of initially stressed bodies. They first wrote the mixed initial boundary value problem within the context of thermoelasticity of initially stressed bodies. Then they established some Lagrange type identities and also introduced the Cesaro means of various parts of the total energy associated to the solutions. Marin and Lupu (1998) obtained a spatial estimate, similar to that of Saint-Venant type by using a measure of Toupin type associated with the corresponding steady-state vibration and assuming that the exciting frequency was lower to a certain critical frequency. Marin (2010) extended the concept of domain of influence in order to cover the elasticity of microstretch materials. Arefi (2015) suggested an analytical solution of a curved beam with different shapes made of functionally graded materials (FGMs). Bennai *et al.* (2015) developed a new refined hyperbolic shear and normal deformation beam theory to study the free vibration and buckling of functionally graded (FG) sandwich beams under various boundary conditions. Bouchafa *et al*. (2015) used refined hyperbolic shear deformation theory (RHSDT) for the thermoelastic bending analysis of functionally graded sandwich plates. Moradi-Dastjerdi and Momeni-Khabisi (2016) studied free and forced vibration of plates reinforced by wavy carbon nanotube. The plates were resting on Winkler-Pasternak elastic foundations and subjected to periodic or impact loading.

Nowadays, the use of carbon nanotubes in polymer/carbon nanotube composites has attracted the attention of many researchers (Wagner *et al.* 1997). A high aspect ratio, low weight of CNTs and their extraordinary mechanical properties (strength and flexibility) provide the ultimate reinforcement for the next generation of extremely lightweight but highly elastic and very strong advanced composite materials. On the other hand, by using of the polymer/CNT composites in advanced composite materials, we can achieve structures with low weight, high strength and high stiffness in many structures of civil, mechanical and space engineering.

Several researches have recently investigated the elastic properties of multiwalled carbon nanotube (MWCNT) and their composites (Fidelus *et al.* 2005, Ghavamian *et al*. 2012). Gojny *et al*. (2005) focused on the evaluation of the different types of the CNTs applied, their influence on the mechanical properties of epoxy-based nanocomposites and the relevance of surface functionalization. Therefore, the study of the mechanical performance of CNT-based composites and the discovery of possible innovative applications has recently attracted the interest of many researchers.

Several researchers have reported that mechanical

properties of polymeric matrices can be drastically increased (Montazeri *et al.* 2010, Yeh *et al*. 2006) by adding a few weight percent (wt%) MWCNTs. Montazeri et al. (2010) showed that modified Halpin-Tsai equation with exponential Aspect ratio can be used to model the experimental result of MWCNT composite samples. They also demonstrated that reduction in Aspect ratio (L/d) and nanotube length cause a decrease in aggregation and above 1.5 wt%, nanotubes agglomerate causing a reduction in Young's modulus values. Thus, it is important to determine the effect Aspect ratio and arrangement of CNTs on the effective properties of carbon nanotube-reinforced composite (CNTRC). Yeh *et al.* (2006) used the Halpin-Tsai equation to show the effect of MWNT shape factor (L/d) on the mechanical properties. They showed that the mechanical properties of nanocomposite samples with the higher shape factor (L/d) values were better than the ones with the lower shape factor. The reinforcement effect of MWCNTs with different aspect ratio in an epoxy matrix has been carried out by Martone *et al.* (2011). They showed that progressive reduction of the tubes effective aspect ratio occurred, because of the increasing connectedness between tubes upon an increase in their concentration. Also they investigated the effect of nanotube curvature on the average contacts number between tubes by means of the waviness that accounts for the deviation from the straight particles assumption.

In structural mechanics, one of the most popular semi-analytical methods is differential quadrature method (DQM) (Bellman and Casti 1971, Tahouneh 2016, Tahouneh and Naei 2014, Tahouneh 2014), remarkable success of which has been demonstrated by many researchers in vibration analysis of plates, shells, and beams. Tornabene *et al*. (2014) studied free vibration of free-form doubly-curved shells made of functionally graded materials using higher-order equivalent single layer theories. The partial differential system of equations was solved by using the Generalized Differential Quadrature (GDQ) method. The recent developments of differential quadrature method as well as its major applications in engineering are discussed in detail in book by Shu (2000). One can compare DQM solution procedure with the other two widely used traditional methods for structural analysis, i.e., Rayleigh-Ritz method and FEM. The main difference between the DQM and the other methods is how the governing equations are discretized. In DQM, the governing equations and boundary conditions are directly discretized, and thus elements of stiffness and mass matrices are evaluated directly. But in Rayleigh-Ritz and FEMs, the weak form of the governing equations should be developed and the boundary conditions are satisfied in the weak form. Generally by doing so larger number of integrals with increasing amount of differentiation should be done to arrive at the element matrices. In addition, the number of degrees of freedom will be increased for an acceptable accuracy. In comparison with research works on the free vibration or buckling analyses of FG structures, only a few references can be found that consider the effect of MWCNT on the vibrational behavior of structures (Heshmati and Yas 2013).

To the author's best knowledge, still very little work has been done for vibration analysis of FG-MWCNT structures. The aim of this study is to fill this apparent gap in this area by providing the 3-D vibration analysis results for FG-MWCNT curved panel with power-law distribution of nanotube. The effective material properties of the FG-MWCNT structures are estimated using the modified Halpin-Tsai equation.

2. Problem description

2.1 Mechanical properties of the cylindrical panel

Consider an FG sandwich curved panel as shown in Fig. 1. A cylindrical coordinate system (*r, θ, z*) is used to label the material point of the panel. In this study, I will discuss about the results in the literature on mechanical properties of polymer nanotube composites.

The Halpin-Tsai equation assumes that the filler are straight and uniform dispersion of the filler in the polymer matrix. The Halpin-Tsai equation (Halpin *et al.* 1969, Affdl Halpin and Kardos 1976) has been recognized for its ability to predict the modulus values for the fiber-reinforced composite samples. Modified Halpin–Tsai equation is proposed to evaluate the Young's modulus and tensile strength of the MWNTs/phenolic composites by adopting an orientation factor and an exponential shape factor in the equation. The effective mechanical properties of the CNTRC panel are obtained based on a modified Halpin-Tsai equation according to (Montazeri *et al*. 2010, Yeh *et al.* 2006)

$$E = E_m \frac{1+\eta_L \eta_T V_{cn}}{1-\eta_T V_{cn}}, \eta_T = \frac{\alpha E_{cn}/E_m - 1}{\alpha E_{cn}/E_m + \eta_L} \quad (1)$$

The effective Young's modulus of MWNT can be deduced from Eq. (1) as follows

$$E_f = \frac{(2l/d + V_{cn})E - 2l/d(1-V_{cn})E_m}{\alpha[(2l/d + V_{cn} + 1)E_m - (1-V_{cn})E]} E_m \quad (2)$$

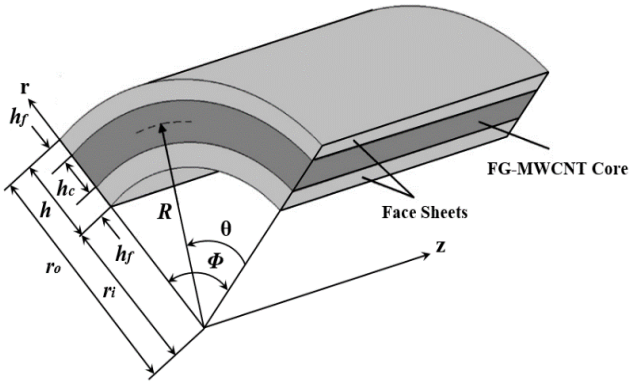

Fig. 1 Geometry and coordinates of the thick sandwich curved panel with FG-MWCNT Core and Face Sheets

From the linear region of the fitting line for MWNTs/phenolic composites, the effective Young's modulus (E_f) of MWCNT is 953 GPa. In above-mentioned equations, l and d are the length and the diameter of CNT and α is CNT orientation efficiency; E_{cn} and E_m are the longitudinal elastic moduli of the MWCNT and pure polymer; V_{cn} is the CNT volume fraction and η_L is the exponential shape factor that can be stated as follows

$$\eta_L = 2\frac{l}{d}e^{-aV_{cn}-b} \tag{3}$$

the exponential shape factor is related to the aspect ratio of reinforcement length l and diameter d in the Halpin-Tsai equation. The exponential shape factor is used to fit the nonlinear region for the MWNTs content over 2.0 wt%. a and b are constants, related to the degree of MWNTs aggregation, which account for the nonlinear behavior of the Halpin-Tsai equation in the MWNTs wt% range considered (Montazeri *et al.* 2010, Yeh *et al.* 2006). The effect of the aggregation-related coefficient a on the model curve is studied by Yeh *et al.* (2006). Larger a tends to soften the fitted curves of Young's modulus of the MWNTs/phenolic composites at high MWNTs additive, which indicate more aggregation initiated with increasing MWNTs content. The effect of the aggregation-related coefficient b on the model curve for Young's modulus of the MWNTs/ phenolic composites is also investigated by Yeh *et al.* (2006). The Young's modulus of composites is further tuned to bend lower for higher values of b at high MWNTs additive. After systematically varying the aggregation-related constants a and b, the Young's modulus of MWNTs/phenolic composites can be modeled by Eq. (1) with exponential shape factor (Eq. (3)).

The resulting effective properties for the randomly oriented MWCNT composite are isotropic, despite the CNTs having transversely isotropic effective properties. When CNTs are completely randomly oriented in the matrix, the composite is then isotropic. In this article, the experimental data for the Young's modulus of MWCNT/phenolic composites with different mass fraction of MWCNTs, reported by Yeh *et al.* (2006), was used to fit the above Halpin-Tsai. In Fig. 2, the predicted Young's moduli using Eq. (1) is shown. The best fit was achieved by taking the model parameters given in Table 1.

Table 1 Material properties for the pure phenolic MWCNTs

Polymer (phenolic)	MWCNTs
E_m=5.13 GPa	E_{cn}=953 GPa,
	ρ_{cn}=1.03 g/ml, υ_{cn}=0.29
	α=1/6, l=17.57 μm,
ρ_m=1.03 g/ml	d=23.63 nm,
υ_m=0.34	a=75, b=1

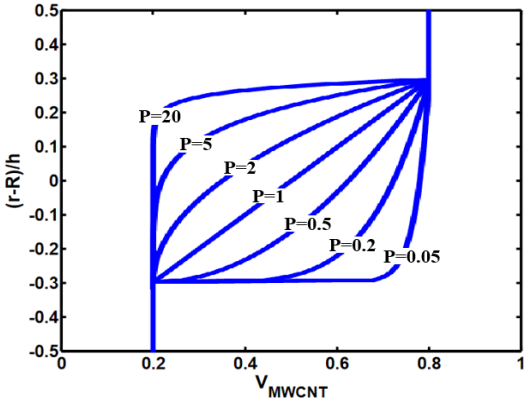

Fig. 3 Variations of the volume fraction of reinforcement (V_{MWCNT}) through the radial direction of curved panel for different values of "p"

Using this prediction model, the Young's modulus of functionally graded MWCNT/phenolic composites will be estimated during the numerical solutions in the next sections. Also, the mass density and Poisson's ratio of the MWCNT/phenolic composite can be calculated according to rule of mixtures, respectively, by

$$\upsilon_{ij} = V_{cn}\upsilon^{cn} + V_m\upsilon^m, ij = 12,13 \text{ and } 23$$
$$\rho = V_{cn}\rho^{cn} + V_m\rho^m \tag{4}$$

where υ^{cn} and ρ^{cn} are Poisson's ratio and density, respectively, of the MWCNT and υ^m and ρ^m are corresponding properties for the matrix. The reinforcement volume fraction of FG-MWCNT panel is assumed as follows (Pelletier Jacob and Vel Senthil 2006)

$$V_{MWCNT} = \begin{cases} V_i, r_i \le r \le r_i + h_f \\ V_i + (V_o - V_i)\left(\frac{r-R}{h_c}\right)^p, r_i + h_f \le r \le r_o - h_f \\ V_o, r_o - h_f \le r \le r_o \end{cases} \tag{5}$$

where V_i and V_o, which have values that range from 0 to 1. The exponent "p" governs the through-thickness fiber volume fraction profile. The through-thickness variations of the volume fractions are depicted in Fig. 3. As shown in Fig. 3, the volume fraction of core varies from 0.2 to 0.8 as η (η =r-R/h) varies from $-h_c/2$ and $h_c/2$ while the reinforcement volume fractions of top and bottom faces are 0.8 and 0.2, respectively.

3. Governing equations

The mechanical constitutive relation that relates the stresses to the strains are as follows

$$\begin{bmatrix} \sigma_r \\ \sigma_\theta \\ \sigma_z \\ \tau_{z\theta} \\ \tau_{rz} \\ \tau_{r\theta} \end{bmatrix} = \begin{bmatrix} C_{11} & C_{12} & C_{13} & 0 & 0 & 0 \\ C_{12} & C_{22} & C_{23} & 0 & 0 & 0 \\ C_{13} & C_{23} & C_{33} & 0 & 0 & 0 \\ 0 & 0 & 0 & C_{44} & 0 & 0 \\ 0 & 0 & 0 & 0 & C_{55} & 0 \\ 0 & 0 & 0 & 0 & 0 & C_{66} \end{bmatrix} \begin{bmatrix} \varepsilon_r \\ \varepsilon_\theta \\ \varepsilon_z \\ \gamma_{z\theta} \\ \gamma_{rz} \\ \gamma_{r\theta} \end{bmatrix} \tag{6}$$

In the absence of body forces, the governing equations are as follows

$$\frac{\partial \sigma_r}{\partial r}+\frac{1}{r}\frac{\partial \tau_{r\theta}}{\partial \theta}+\frac{\partial \tau_{rz}}{\partial z}+\frac{\sigma_r-\sigma_\theta}{r}=\rho\frac{\partial^2 u_r}{\partial t^2},$$
$$\frac{\partial \tau_{r\theta}}{\partial r}+\frac{1}{r}\frac{\partial \sigma_\theta}{\partial \theta}+\frac{\partial \tau_{\theta z}}{\partial z}+\frac{2\tau_{r\theta}}{r}=\rho\frac{\partial^2 u_\theta}{\partial t^2}, \quad (7)$$
$$\frac{\partial \tau_{rz}}{\partial r}+\frac{1}{r}\frac{\partial \tau_{\theta z}}{\partial \theta}+\frac{\partial \sigma_z}{\partial z}+\frac{\tau_{rz}}{r}=\rho\frac{\partial^2 u_z}{\partial t^2}$$

Strain-displacement relations are expressed as

$$\varepsilon_r=\frac{\partial u_r}{\partial r},\varepsilon_\theta=\frac{u_r}{r}+\frac{1}{r}\frac{\partial u_\theta}{\partial \theta},\varepsilon_z=\frac{\partial u_z}{\partial z},$$
$$\gamma_{\theta z}=\frac{\partial u_\theta}{\partial z}+\frac{1}{r}\frac{\partial u_z}{\partial \theta},\gamma_{rz}=\frac{\partial u_r}{\partial z}+\frac{\partial u_z}{\partial r}, \quad (8)$$
$$\gamma_{r\theta}=\frac{1}{r}\frac{\partial u_r}{\partial \theta}+\frac{\partial u_\theta}{\partial r}-\frac{u_\theta}{r}$$

where u_r , u_θ and u_z are radial, circumferential and axial displacement components, respectively. Upon substitution Eq. (8) into (6) and then into (7), the equations of motion in terms of displacement components with infinitesimal deformations can be written as

$$\begin{bmatrix} F_{1r} & F_{1\theta} & F_{1z} \\ F_{2r} & F_{2\theta} & F_{2z} \\ F_{3r} & F_{3\theta} & F_{3z} \end{bmatrix}\begin{Bmatrix} u_r \\ u_\theta \\ u_z \end{Bmatrix}=\begin{Bmatrix} \rho\frac{\partial^2 u_r}{\partial t^2} \\ \rho\frac{\partial^2 u_\theta}{\partial t^2} \\ \rho\frac{\partial^2 u_z}{\partial t^2} \end{Bmatrix} \quad (9)$$

where coefficients F_{ij} are given in Appendix. The boundary conditions at the concave and convex surfaces, $r=r_i$ and r_o, respectively, can be described as follows

$$\tau_{rz}=\tau_{r\theta}=0,\sigma_r=0 \quad (10)$$

In this investigation, three different types of classical boundary conditions at edges z=0 and L_z of the finite panel can be stated as follows:

-Simply supported (S)

$$U_r=U_\theta=\sigma_z=0 \quad (11)$$

-Clamped (C):

$$U_r=U_\theta=U_z=0 \quad (12)$$

-Free (F):

$$\sigma_z=\sigma_{z\theta}=\sigma_{zr}=0 \quad (13)$$

4. Solution procedure

4.1 DQM solution for equations of motion and boundary conditions

It is necessary to develop appropriate methods to investigate the mechanical responses of sandwich structures. But, due to the complexity of the problem, it is difficult to obtain the exact solution. In this paper, the differential quadrature method (DQM) approach is used to solve the governing equations of sandwich curved panel. One can compare the DQM solution procedure with the other two widely used traditional methods for plate analysis, i.e., Rayleigh-Ritz method and FEM. The main difference between the DQM and the other methods is how the governing equations are discretized. In DQM the governing equations and boundary conditions are directly discretized, and thus elements of stiffness and mass matrices are evaluated directly. But in Rayleigh-Ritz and FEMs, the weak form of the governing equations should be developed and the boundary conditions are satisfied in the weak form. Generally by doing so larger number of integrals with increasing amount of differentiation should be done to arrive at the element matrices. Also, the number of degrees of freedom will be increased for an acceptable accuracy.

In Generalized Differential Quadrature Method (GDQM), the *n*th order partial derivative of a continuous function $f(x,z)$ with respect to x at a given point x_i can be approximated as a linear summation of weighted function values at all the discrete points in the domain of *x*, that is

$$\frac{\partial^n f_{(x_i,z)}}{\partial x^n}=\sum_{k=1}^{N} q_{ik}^n f_{(x_{ik},z)} \quad (i=1,2,...,N,n=1,2,...,N-1) \quad (14)$$

where *N* is the number of sampling points and q_{ij}^n is the x^i dependent weight coefficient. To determine the weighting coefficients q_{ij}^n, the Lagrange interpolation basic functions are used as the test functions, and explicit formulas for computing these weighting coefficients can be obtained as (Shu 2000)

$$q_{ij}^{(1)}=\frac{M^{(1)}(x_i)}{(x_i-x_j)M^{(1)}(x_j)},i,j=1,2,...,N,i\neq j \quad (15)$$

where

$$M^{(1)}(x_i)=\prod_{j=1,i\neq j}^{N}(x_i-x_j) \quad (16)$$

and for higher order derivatives, one can use the following relations iteratively

$$q_{ij}^{(n)}=n(q_{ii}^{(n-1)}q_{ij}^{1}-\frac{q_{ij}^{(n-1)}}{(x_i-x_j)}),\ i,j=1,2,...,N, \quad (17)$$
$$i\neq j,n=2,3,...,N-1$$

$$q_{ii}^{(n)}=-\sum_{j=1,i\neq j}^{N} q_{ij}^{(n)} \quad i=1,2,...,N,\ n=1,2,...,N-1 \quad (18)$$

A simple and natural choice of the grid distribution is the uniform grid-spacing rule. However, it was found that non-uniform grid-spacing yields result with better accuracy. Hence, in this work, the Chebyshev-Gauss-Lobatto quadrature points are used

$$x_i=\frac{1}{2}(1-\cos(\frac{i-1}{N-1}\pi)) \quad i=1,2,...,N \quad (19)$$

4.2 Discretization procedure

For the curved panels with simply supported at one pair of opposite edges, the displacement components can be expanded in terms of trigonometric functions in the direction normal to these edges. In this work, it is assumed that the edges θ=0 and θ=Φ are simply supported. Hence

$$\begin{aligned} u_r(r,\theta,z,t) &= \sum_{m=1}^{\infty} U_r(r,z)\sin(\frac{m\pi}{\Phi}\theta)e^{i\omega t}, \\ u_\theta(r,\theta,z,t) &= \sum_{m=1}^{\infty} U_\theta(r,z)\cos(\frac{m\pi}{\Phi}\theta)e^{i\omega t}, \\ u_z(r,\theta,z,t) &= \sum_{m=1}^{\infty} U_z(r,z)\sin(\frac{m\pi}{\Phi}\theta)e^{i\omega t} \end{aligned} \tag{20}$$

where m is the circumferential wave number, ω is the natural frequency and i ($=\sqrt{-1}$) is the imaginary number. Substituting for displacement components from Eq. (20) into Eq. (9), and then using GDQ method to discretize the equations of motion, one can get the following equations:

$$\begin{aligned} &(c_{11})_{ij}\sum_{n=1}^{N_r} B_{in}^r U_{rnj} + (c_{12})_{ij}(\frac{m\pi}{\Phi r_i^2}U_{\theta ij} - \\ &\frac{m\pi}{\Phi r_i}\sum_{n=1}^{N_r} A_{in}^r U_{\theta nj} + \frac{1}{r_i}\sum_{n=1}^{N_r} A_{in}^r U_{rnj} - \frac{U_{rij}}{r_i^2}) + \\ &(c_{13})_{ij}\sum_{n=1}^{N_r}\sum_{v=1}^{N_z} A_{jv}^z A_{in}^r U_{znv} + (\frac{\partial c_{11}}{\partial r})_{ij}\sum_{n=1}^{N_r} A_{in}^r U_{rnj} \\ &+(\frac{\partial c_{12}}{\partial r})_{ij}(\frac{1}{r_i}U_{rij} - \frac{m\pi}{\Phi r_i}U_{\theta ij}) + (\frac{\partial c_{13}}{\partial r})_{ij}\sum_{n=1}^{N_z} A_{jn}^z U_{zin} \\ &+\frac{(c_{66})_{ij}}{r_i}(-\frac{m\pi}{\Phi}\sum_{n=1}^{N_r} A_{in}^r U_{\theta nj} - \frac{1}{r_i}(\frac{m\pi}{\Phi})^2 U_{rij} \\ &+\frac{m\pi}{\Phi r_i}U_{\theta ij}) + (c_{55})_{ij}(\sum_{n=1}^{N_z} B_{jn}^z U_{rin} \\ &+\sum_{n=1}^{N_r}\sum_{v=1}^{N_z} A_{jv}^z A_{in}^r U_{znv}) + \frac{1}{r_i}((c_{11})_{ij}\sum_{n=1}^{N_r} A_{in}^r U_{rnj} \\ &+(c_{12})_{ij}(\frac{U_{rij}}{r_i} - \frac{m\pi}{\Phi r_i}U_{\theta ij}) + (c_{13})_{ij}\sum_{n=1}^{N_z} A_{jn}^z U_{zin} \\ &-(c_{12})_{ij}\sum_{n=1}^{N_r} A_{in}^r U_{rnj} - (c_{22})_{ij}(\frac{U_{rij}}{r_i} - \frac{m\pi}{\Phi r_i}U_{\theta ij}) \\ &-(c_{23})_{ij}\sum_{n=1}^{N_z} A_{jn}^z U_{zin}) = -\rho_{ij}\omega^2 U_{rij} \end{aligned} \tag{21}$$

$$\begin{aligned} &(c_{66})_{ij}(-\frac{1}{r_i^2}\frac{m\pi}{\Phi}U_{rij} + \frac{m\pi}{\Phi r_i}\sum_{n=1}^{N_r} A_{in}^r U_{rnj} + \\ &\sum_{n=1}^{N_r} B_{in}^r U_{\theta nj} + \frac{U_{\theta ij}}{r_i^2} - \frac{1}{r_i}\sum_{n=1}^{N_r} A_{in}^r U_{\theta nj}) \\ &+(\frac{\partial c_{66}}{\partial r})_{ij}(\frac{m\pi}{\Phi r_i}U_{rij} + \sum_{n=1}^{N_r} A_{in}^r U_{\theta nj} - \frac{U_{\theta ij}}{r_i}) \\ &+\frac{1}{r_i}((c_{12})_{ij}\frac{m\pi}{\Phi}\sum_{n=1}^{N_r} A_{in}^r U_{rnj} + (c_{22})_{ij} \\ &(\frac{m\pi}{\Phi r_i}U_{rij} - \frac{1}{r_i}(\frac{m\pi}{\Phi})^2 U_{\theta ij}) + (c_{23})_{ij} \\ &\frac{m\pi}{\Phi}\sum_{n=1}^{N_z} A_{jn}^z U_{zin}) + (c_{44})_{ij}(\sum_{n=1}^{N_z} B_{jn}^z U_{\theta in} + \\ &\frac{m\pi}{\Phi r_i}\sum_{n=1}^{N_z} A_{jn}^z U_{zin}) + \frac{2(c_{66})_{ij}}{r_i}(\frac{m\pi}{\Phi r_i}U_{rij} + \\ &\sum_{n=1}^{N_r} A_{in}^r U_{\theta nj} - \frac{U_{\theta ij}}{r_i}) = -\rho_{ij}\omega^2 U_{\theta ij} \end{aligned}$$

$$\begin{aligned} &(c_{55})_{ij}(\sum_{n=1}^{N_r}\sum_{v=1}^{N_z} A_{jv}^z A_{in}^r U_{rnv} + \sum_{n=1}^{N_r} B_{in}^r U_{znj}) + \\ &(\frac{\partial c_{55}}{\partial r})_{ij}(\sum_{n=1}^{N_z} A_{jn}^z U_{rin} + \sum_{n=1}^{N_r} A_{in}^r U_{znj}) + \frac{(c_{44})_{ij}}{r_i} \\ &(-\frac{m\pi}{\Phi}\sum_{n=1}^{N_z} A_{jn}^z U_{\theta in} - \frac{1}{r_i}(\frac{m\pi}{\Phi})^2 U_{zij}) + \\ &(c_{13})_{ij}\sum_{n=1}^{N_r}\sum_{v=1}^{N_z} A_{jv}^z A_{in}^r U_{rnv} + (c_{23})_{ij}(\frac{1}{r_i}\sum_{n=1}^{N_z} A_{jn}^z U_{rin} - \\ &\frac{m\pi}{\Phi r_i}\sum_{n=1}^{N_z} A_{jn}^z U_{\theta in}) + (c_{33})_{ij}\sum_{n=1}^{N_z} B_{jn}^z U_{zin} + \frac{(c_{55})_{ij}}{r_i} \\ &(\sum_{n=1}^{N_z} A_{jn}^z U_{rin} + \sum_{n=1}^{N_r} A_{in}^r U_{znj}) = -\rho_{ij}\omega^2 U_{zij} \end{aligned} \tag{23}$$

In the above-mentioned equations i=2…, N_{r-1} and j=2,.., N_{z-1}. A_{ij}^r, A_{ij}^z and B_{ij}^r, B_{ij}^z are the first and second order GDQ weighting coefficients in the r- and z-directions, respectively. Substituting for displacement components from Eq. (14) into Eq. (10), and then using GDQ method to discretize the boundary conditions, one can get the following equations:

Eq. (10)

$$\begin{aligned} &\sum_{n=1}^{N_z} A_{jn}^z U_{rin} + \sum_{n=1}^{N_r} A_{in}^r U_{znj} = 0, \\ &\frac{m\pi}{\Phi r_i}U_{rij} + \sum_{n=1}^{N_r} A_{in}^r U_{\theta nj} - \frac{U_{\theta ij}}{r_i} = 0, \\ &(c_{11})_{ij}\sum_{n=1}^{N_r} A_{in}^r U_{rnj} + (c_{12})_{ij}(\frac{U_{rij}}{r_i} - \frac{m\pi}{\Phi r_i}U_{\theta ij}) \\ &+(c_{13})_{ij}\sum_{n=1}^{N_z} A_{jn}^z U_{zin} = 0 \end{aligned} \tag{24}$$

where i=1 at r=r_i and i=N_r at r=r_o, and j=1,2,…,N_z. By following the same procedure the boundary conditions at z=0 and L_z stated in Eqs. (11)-(13), become

Eq. (11)

$$U_{rij} = U_{\theta ij} = 0,$$

$$(c_{13})_{ij} \sum_{n=1}^{N_r} A_{in}^{r} U_{rnj} + (c_{23})_{ij} \left(\frac{U_{rij}}{r_i} - \frac{m\pi}{\Phi r_i} U_{\theta ij}\right) + (c_{33})_{ij} \sum_{n=1}^{N_z} A_{jn}^{z} U_{zin} = 0 \tag{25}$$

Eq. (12)

$$U_{rij} = U_{\theta ij} = U_{zij} 0 \tag{26}$$

Eq. (13)

$$\begin{aligned} &(c_{13})_{ij} \sum_{n=1}^{N_r} A_{in}^{r} U_{rnj} + (c_{23})_{ij} \left(\frac{U_{rij}}{r_i} - \frac{m\pi}{\Phi r_i} U_{\theta ij}\right) \\ &+ (c_{33})_{ij} \sum_{n=1}^{N_z} A_{jn}^{z} U_{zin} = 0, \\ &\sum_{n=1}^{N_z} A_{jn}^{z} U_{\theta in} + \frac{m\pi}{\Phi r_i} U_{zij} = 0, \\ &\sum_{n=1}^{N_z} A_{jn}^{z} U_{rin} + \sum_{n=1}^{N_r} A_{in}^{r} U_{znj} = 0 \end{aligned} \tag{27}$$

In the above equations i=2,…,N_{r-1}; also j=1 at z=0 and j=N_z at z=L_z. In order to carry out the eigenvalue analysis, the domain and boundary nodal displacements should be separated. In vector forms, they are denoted as $\{U_d\}$ and $\{U_b\}$, respectively. Based on this definition, the discretized form of the equations of motion and the related boundary conditions can be represented in the matrix form as

$$\begin{bmatrix} [A_{bb}] & [A_{bd}] \\ [A_{db}] & [A_{dd}] \end{bmatrix} \begin{Bmatrix} \{U_b\} \\ \{U_d\} \end{Bmatrix} = \begin{Bmatrix} \{0\} \\ -\omega^2 [M] \{U_d\} \end{Bmatrix} \tag{28}$$

Where $\{U_d\}$ and $\{U_b\}$ are as follows

$$\begin{aligned} \{U_d\} &= \left\{ \{U_{rd}\}, \{U_{\theta d}\}, \{U_{zd}\} \right\}^T, \\ \{U_b\} &= \left\{ \{U_{rb}\}, \{U_{\theta b}\}, \{U_{zb}\} \right\}^T \end{aligned} \tag{29}$$

In relations 28 and 29, subscripts b and d correspond to the displacement vectors at boundaries and domain of the panel, respectively. Eliminating the boundary degrees of freedom, Eq. (28) becomes

$$\left([A] + \omega^2 [M] \{U_d\} \right) = \{0\} \tag{30}$$

where $[A] = [A_{dd}] - [A_{db}][A_{bb}]^{-1}[A_{bd}]$. The above eigenvalue system of equations can be solved to find the natural frequencies and mode shapes of the curved panel.

5. Numerical results and discussion

To verify the proficiency of presented method and three-parameter model for volume fraction of FG materials, several numerical examples are carried out for comparisons. The results of the presented formulations are given in the form of convergence studies with respect to N_r and N_z, the number of discrete points distributed along the radial and axial directions, respectively. To validate the proposed approach its convergence and accuracy are demonstrated via different examples. The obtained natural frequencies based on the three-dimensional elasticity formulation are compared with those of the power series expansion method for FG curved panels (Pradyumna and Bandyopadhyay 2008, Matsunaga 2008). In these studies the material properties of functionally graded materials are assumed as follows-Metal (Aluminum, Al): E_m=70*10^9 Pa, ρ_m=2702 Kg/m^3, υ_m=0.3-Ceramic (Alumina, Al_2O_3): E_c=380*10^9 Pa, ρ_c=3800 Kg/m^3, υ_c=0.3 Subscripts m and c refer to the metal and ceramic constituents which denote the material properties of the outer and inner surfaces of the panel, respectively. To validate the analysis, results for FG cylindrical shells are compared with similar ones in the literature, as shown in Table 2.

As observed, there is a good agreement between the results. Besides fast rate of convergence of the method is quite evident, and it is found that only thirteen grid points (Nr=Nz=13) along the radial and axial directions can yield accurate results. Further validation of the present results for isotropic FG cylindrical panel is shown in Table 3. In this Table, comparison is made for different Lz/R and Lz/h ratios, and as it is observed there is also a good agreement between the results.

After demonstrating the convergence and accuracy of the present method, parametric studies for 3-D vibration analysis of thick FG-MWCNT sandwich curved panels with considering a power-law distribution, thickness-to-mean radius ratio and different combinations of Free, Simply supported and Clamped boundary conditions of the curved panel, are computed. It should be noted that two opposite axial edges are simply supported while any arbitrary boundary conditions including Free, Simply supported and Clamped are applied to the curved edges.

The non-dimensional natural frequency can be assumed as follows

$$\Omega = \omega h \sqrt{\rho_i / E_i} \tag{31}$$

Where ρ_i and E_i are mechanical properties of MWCNT.

The effect of length-to-mean radius ratio of the sandwich panel with four edges simply supported on the non-dimensional natural frequency is shown in Fig. 4. It shows that the non-dimensional natural frequency decreases with the increase of L_z/R ratio and then remains almost unaltered for L_z/R greater than 8. It should be noted that this behavior is also observed at other boundary conditions, but, for the sale of brevity, we consider only this type of boundary condition here. The influence of the panel angle on the non-dimensional natural frequency parameter of the laminated structure is depicted in Fig. 5. This figure shows that at first the non-dimensional natural frequency parameter decreases sharply, but, by increasing the panel angle it increases very slowly and remains somehow unaltered. The effects of thickness-to-mean radius ratio on the non-dimensional natural frequency parameters of FG-MWCNT curved panel for different types of boundary conditions are shown in Fig. 6.

Table 2 Comparison of the normalized natural frequency of an FGM composite curved panel with four edges simply supported

P (volum fraction index)		R/L_z				
		0.5	1	5	10	50
0	$N_r=N_z=5$	69.9774	52.1052	42.7202	42.3717	42.2595
	$N_r=N_z=7$	69.9722	52.1052	42.7158	42.3718	42.2550
	$N_r=N_z=9$	69.9698	52.1003	42.7159	42.3700	42.2553
	$N_r=N_z=11$	69.9700	52.1003	42.7160	42.3677	42.2552
	$N_r=N_z=13$	69.9700	52.1003	42.7160	42.3677	42.2553
	Pradyumna and Bandyopadhyay (2008)	68.8645	51.5216	42.2543	41.908	41.7963
0.2	$N_r=N_z=5$	65.1470	47.9393	39.1282	38.8010	38.7020
	$N_r=N_z=7$	65.4449	48.0456	39.1008	38.7366	38.6834
	$N_r=N_z=9$	65.4526	48.1340	39.0836	38.7568	38.6581
	$N_r=N_z=11$	65.4304	48.1340	39.0835	38.7568	38.6580
	$N_r=N_z=13$	65.4304	48.1340	39.0835	38.7568	38.6581
	Pradyumna and Bandyopadhyay (2008)	64.4001	47.5968	40.1621	39.8472	39.7465
0.5	$N_r=N_z=5$	60.1196	43.5539	36.1264	35.8202	34.7341
	$N_r=N_z=7$	60.2769	43.7128	36.1401	35.7964	35.0677
	$N_r=N_z=9$	60.3574	43.7689	36.0944	35.7890	35.7032
	$N_r=N_z=11$	60.3574	43.7688	36.0943	35.7891	35.7032
	$N_r=N_z=13$	60.3574	43.7689	36.0944	35.7891	35.7032
	Pradyumna and Bandyopadhyay (2008)	59.4396	43.3019	37.287	36.9995	36.9088
1	$N_r=N_z=5$	54.1034	38.5180	31.9860	30.7065	30.6336
	$N_r=N_z=7$	54.6039	39.1477	32.1140	31.6982	31.5397
	$N_r=N_z=9$	54.7141	39.1620	32.0401	31.7608	31.6877
	$N_r=N_z=11$	54.7141	39.1621	32.0401	31.7608	31.6878
	Nr=Nz=13	54.7141	39.1621	32.0401	31.7608	31.6877
	Pradyumna and Bandyopadhyay (2008)	53.9296	38.7715	33.2268	32.9585	32.875
2	$N_r=N_z=5$	46.9016	34.7702	27.6657	27.4295	27.3725
	$N_r=N_z=7$	47.9865	34.6980	27.5733	27.3389	27.2669
	$N_r=N_z=9$	48.5250	34.6852	27.5614	27.3238	27.2663
	$N_r=N_z=11$	48.5250	34.6851	27.5614	27.3239	27.2663
	$N_r=N_z=13$	48.5250	34.6851	27.5614	27.3239	27.2662
	Pradyumna and Bandyopadhyay (2008)	47.8259	34.3338	27.4449	27.1789	27.0961

One can see that with the increase of thickness-to-mean radius ratio, the non-dimensional natural frequency parameter increasing and this behavior can be seen in different types of boundary condition.

The effect of material graded index (p) on the non-dimensional natural frequency parameters of curved panel isdepicted in above-mentioned figure.

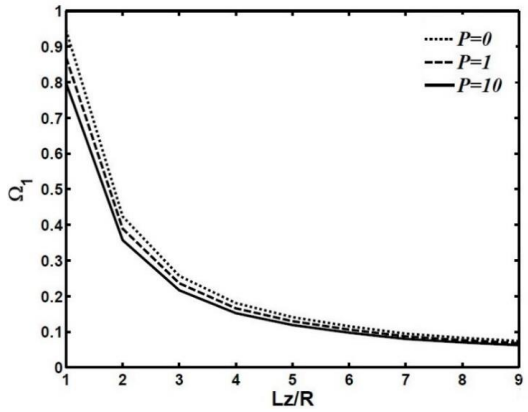

Fig. 4 The effect of length-to-mean radius ratio and material graded index (p) on the fundamental frequency parameter of the FG-MWCNT sandwich curved panel with four edges simply supported (h/R=0.3, Φ=120°)

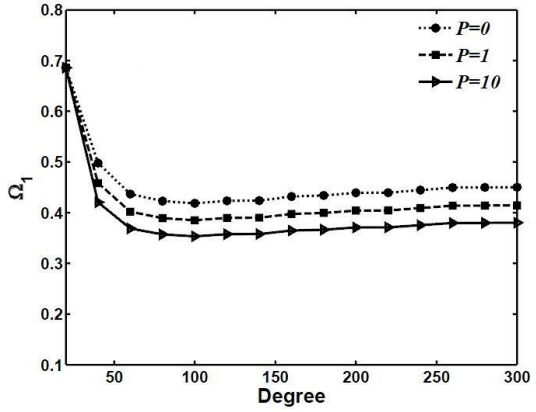

Fig. 5 The effect of the panel angle and material graded index (p) on the fundamental frequency parameter of the FG-MWCNT sandwich curved panel with four edges simply supported (L_z/R=1, h/R=0.3)

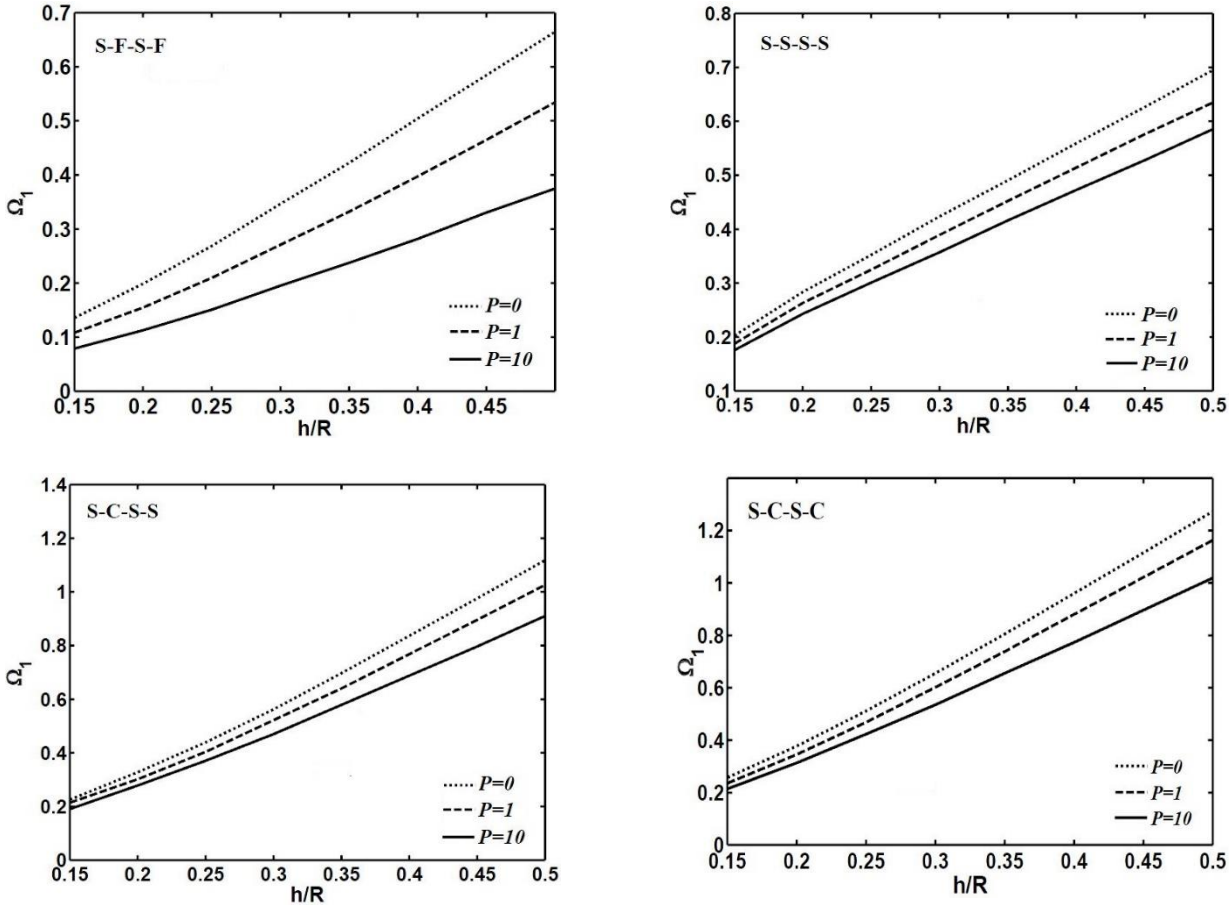

Fig. 6 The effect of thickness-to-mean radius ratios and material graded index (p) on the fundamental frequency parameter of the FG-MWCNT sandwich curved panel with different boundary conditions (L_z/R=1, Φ=120°).

These figures show that for a certain boundary condition the discrepancy between branches steadily increasing as the thickness-to-mean radius ratio is changing from 0.15 to 0.5. It is also seen that for large amount of parameter "P", increasing this parameter does not have significant effect on the non-dimensional natural frequency parameters of FG-MWCNT curved panel.

Results show that S-C-S-C panel has the highest, whereas the S-F-S-F one has the lowest non-dimensional natural frequency parameters, it means that the greater supporting rigidity will lead to higher amount of non-dimensional natural frequency parameter.

In the following discussion, we turn our attention to investigation of the distributions of normalized modal radial, circumferential and axial (T_z=z/L_z) displacements associated with the natural frequencies for FG curved panels. The modal displacement (u_r, u_θ, u_z) of the FG curved panels in vibration is normalized by dividing its maximum absolute value, denoted by (U_{rr}, $U_{\theta\theta}$, U_{zz}). The through-the-length variation of the mode shape of the non-dimensional radial displacement for S-C-S-S and S-C-S-C curved panels with respect to different values of mid-radius to thickness ratio (R/h) is plotted in Figs. 7 and 8 corresponding to the first vibrating mode (m,s)=(1,1).

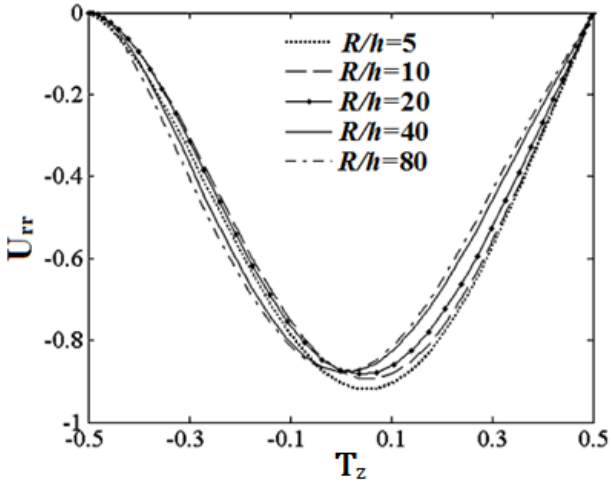

Fig. 7 The effect of R/h ratio on the mode shape of radial displacement of S-C-S-S curved panel ($\Phi=\pi/2$, (m,s)=(1,1))

Table 3 Comparison of the normalized natural frequency of an FGM composite curved panel for various L_Z/R and L_Z/h ratios

			P (volume fraction index)				
			0	0.5	1	4	10
$L_Z/h=2$		$L_Z/R=0.5$					
	Matsunaga (2008)		0.9334	0.8213	0.7483	0.6011	0.5461
	$N_r=N_z=5$		0.9342	0.8001	0.7149	0.5878	0.5133
	$N_r=N_z=7$		0.9249	0.8011	0.7250	0.5783	0.5298
	$N_r=N_z=9$		0.9250	0.8018	0.7253	0.5790	0.5301
	$N_r=N_z=11$		0.9249	0.8017	0.7253	0.5789	0.5300
	$N_r=N_z=13$		0.9250	0.8018	0.7252	0.5790	0.5301
	Matsunaga (2008)	$L_Z/R=1$	0.9163	0.8105	0.7411	0.5967	0.5392
	$N_r=N_z=5$		0.8942	0.7531	0.6746	0.5741	0.4913
	$N_r=N_z=7$		0.8851	0.7671	0.6912	0.5599	0.5074
	$N_r=N_z=9$		0.8857	0.7666	0.6935	0.5531	0.5065
	Nr=Nz=11		0.8857	0.7667	0.6934	0.5531	0.5063
	$N_r=N_z=13$		0.8856	0.7667	0.6935	0.5532	0.5064
$L_Z/h=5$		$L_Z/R=0.5$					
	Matsunaga (2008)		0.2153	0.1855	0.1678	0.1413	0.1328
	$N_r=N_z=5$		0.2230	0.1997	0.1542	0.1374	0.1373
	$N_r=N_z=7$		0.2176	0.1823	0.1624	0.1362	0.1233
	$N_r=N_z=9$		0.2130	0.1817	0.1639	0.1374	0.1296
	$N_r=N_z=11$		0.2128	0.1816	0.1640	0.1377	0.1296
	$N_r=N_z=13$		0.2129	0.1817	0.1640	0.1374	0.1295
	Matsunaga (2008)	$L_Z/R=1$	0.2239	0.1945	0.1769	0.1483	0.1385
	$N_r=N_z=5$		0.2066	0.1765	0.1567	0.1476	0.1409
	$N_r=N_z=7$		0.2133	0.1843	0.1688	0.1377	0.1288
	$N_r=N_z=9$		0.2154	0.1848	0.1671	0.1392	0.1301
	$N_r=N_z=11$		0.2155	0.1847	0.1675	0.1392	0.1299
	$N_r=N_z=13$		0.2155	0.1847	0.1671	0.1392	0.1302

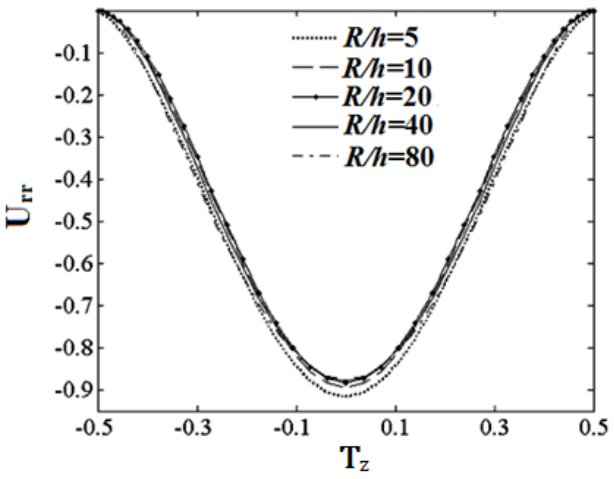

Fig. 8 The effect of R/h ratio on the mode shape of radial displacement of S-C-S-C curved panel ($\Phi=\pi/2$, (m,s)=(1,1))

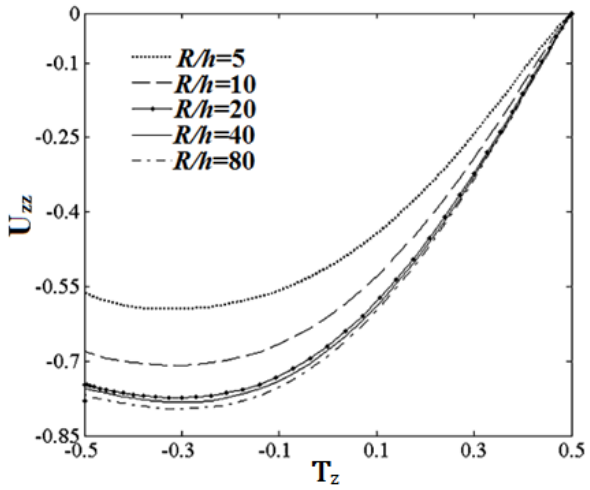

Fig. 9 The effect of R/h ratio on the mode shape of axial displacement of S-F-S-C curved panels ($\Phi=\pi/2$)

Figs. 9 and 10 present the effect of the R/h ratio on the mode shape of the axial displacement of S-F-S-C and S-C-S-C curved panel, respectively. The second and third mode shape of axial displacement of S-C-S-C curved panel are also depicted in Figs. 11 and 12.

Figs. 13-15 present the effect of R/h ratio on the first three mode shapes of circumferential displacement of S-C-S-C curved panel.

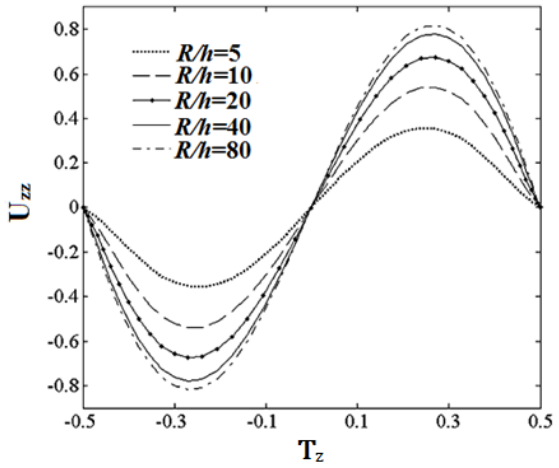

Fig. 10 The effect of R/h ratio on the mode shape of axial displacement of S-C-S-C curved panels (Φ=π/2)

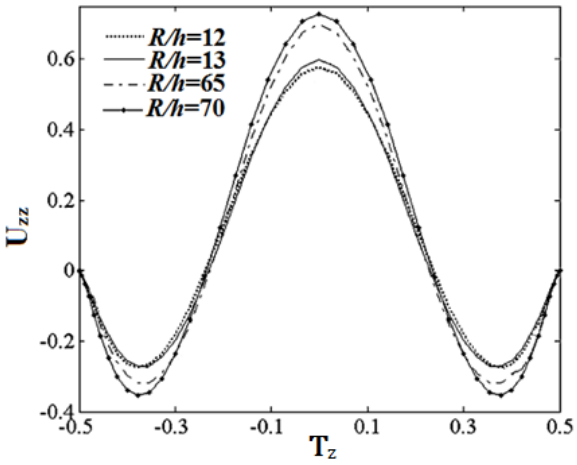

Fig. 11 The effect of R/h ratio on the mode shape of axial displacement of S-C-S-C curved panel (Φ=π/2, (m,s)=(1,2))

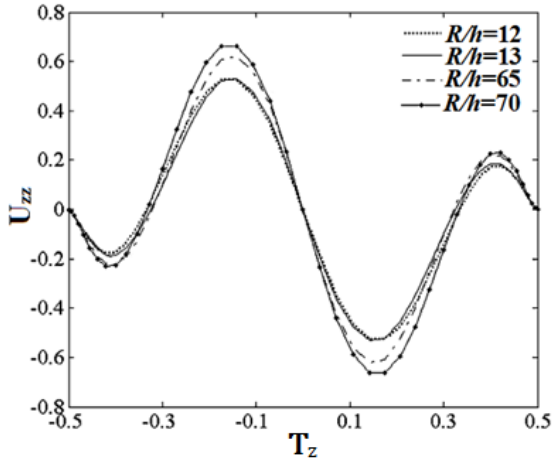

Fig. 12 The effect of R/h ratio on the mode shape of axial displacement of S-C-S-C curved panel (Φ=π/2, (m,s)=(1,3))

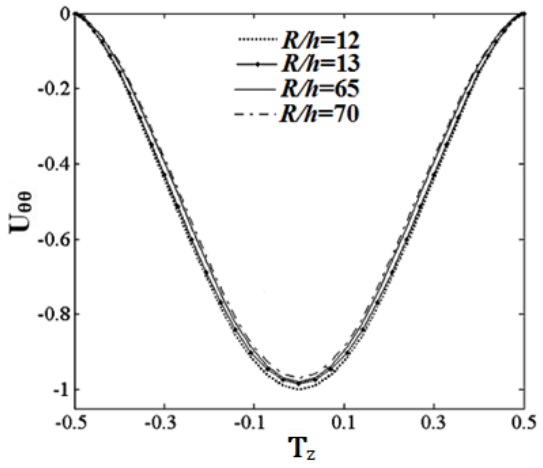

Fig. 13 The effect of R/h ratio on the mode shape of the circumferential displacement of of S-C-S-C curved panel (Φ=π/2, (m,s)=(1,1))

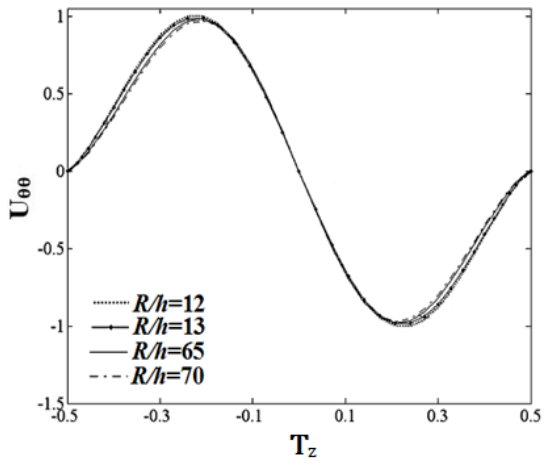

Fig. 14 The effect of R/h ratio on the mode shape of the circumferential displacement of of S-C-S-C curved panel (Φ=π/2, (m,s)=(1,2))

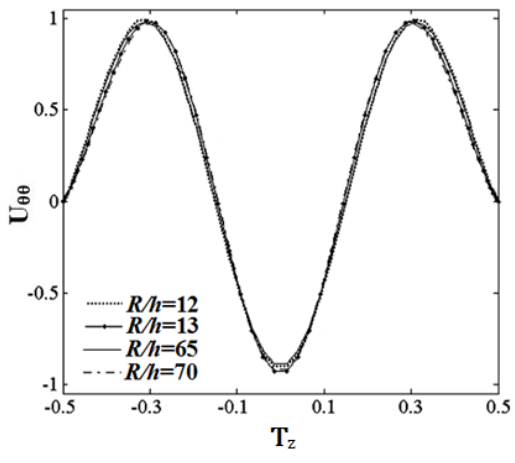

Fig. 15 The effect of R/h ratio on the mode shape of the circumferential displacement of of S-C-S-C curved panel (Φ=π/2, (m,s)=(1,3))

6. Conclusions

In this research work, free vibration of continuous grading sandwich MWCNT curved panels is investigated based on three-dimensional theory of elasticity. Three complicated equations of motion for the panel under consideration are semi-analytically solved by using 2-D differential quadrature method. Using the 2-D differential quadrature method in the r- and z-directions, allows one to deal with sandwich panel with arbitrary thickness distribution of material properties and also to implement the effects of different boundary conditions of the sandwich curved panel efficiently and in an exact manner. The fast rate of convergence and accuracy of the method are investigated through the different solved examples.

The effects of different geometrical parameters such as the thickness-to-mean radius ratio, boundary conditions and material profiles on the performance of the natural frequency parameters of the FG-MWCNT sandwich curved panel are investigated. The main contribution of this work is to present useful results for continuous grading of MWCNT reinforcement in the radial direction of the sandwich panel.
From this study, some conclusions can be made:

- One can see that with the increase of thickness-to-mean radius ratio, the non-dimensional natural frequency parameter increasing and this behavior can be seen in different types of boundary condition.
- Results show that S-C-S-C panel has the highest, whereas the S-F-S-F one has the lowest non-dimensional natural frequency parameters.
- Results reveal that for a certain boundary condition the discrepancy between branches steadily increasing as the thickness-to-mean radius ratio is changing from 0.15 to 0.5.
- It is also seen that for large amount of parameter "P", increasing this parameter does not have significant effect on the non-dimensional natural frequency parameters of FG-MWCNT curved panel.
- It is observed that the non-dimensional natural frequency decreases with the increase L_z/R ratio and then remains almost unaltered for L_z/R greater than 8.
- It is also seen that at first the non-dimensional natural frequency parameter decreases sharply, but, with increasing the panel angle it increases very slowly and remains somehow unaltered.

References

Abrate, S. (1998), "Impact on composite structures", Cambridge UK: Cambridge University Press.

Affdl Halpin, J.C. and Kardos, J.L. (1976), "The Halpin-Tsai equations: A review", *Polym. Eng. Sci.*, **16**(5), 344-352.

Anderson, T.A. (2003), "3D elasticity solution for a sandwich composite with functionally graded core subjected to transverse loading by a rigid sphere", *Compos. Struct.*, **60**(3), 265-274.

Arefi, M. (2015), "Elastic solution of a curved beam made of functionally graded materials with different cross sections", *Steel Compos. Struct.*, **18**(3), 659-672.

Barka, M., Benrahou, K.H., Bakora, A. and Tounsi, A. (2016), "Thermal post-buckling behavior of imperfect temperature-dependent sandwich FGM plates resting on Pasternak elastic foundation", *Steel Compos. Struct.*, **22**(1), 91-112.

Bellman, R. and Casti, J. (1971), "Differential quadrature and long term integration", *J. Math. Anal. Appl.*, **34**(2), 235-238.

Bennai, R., Ait Atmane, H. and Tounsi, A. (2015), "A new higher-order shear and normal deformation theory for functionally graded sandwich beams", *Steel Compos. Struct.*,, **19**(3), 521-546.

Bouchafa, A., Bouiadjra, M.B., Houari, M.S.A. and Tounsi, A. (2015), "Thermal stresses and deflections of functionally graded sandwich plates using a new refined hyperbolic shear deformation theory", *Steel Compos. Struct.*, **18**(6), 1493-1515.

Bouguenina, O., Belakhdar, K., Tounsi, A. and Bedia, E.A.A. (2015), "Numerical analysis of FGM plates with variable thickness subjected to thermal buckling", *Steel Compos. Struct.*, **19**(3), 679-695.

Brischetto, S., Tornabene, F., Fantuzzi, N. and Bacciocchi, M. (2015), "Refined 2D and exact 3D shell models for the free vibration analysis of single- and double-walled carbon nanotubes", *Technologies*, **3**(4), 259-284.

Cai, J.B., Chen W.Q., Ye, G.R. and Ding, H.J. (2000), "On natural frequencies of a transversely isotropic cylindrical panel on a kerr foundation", *J. Sound Vib.*, **232**(5), 997-1004.

Chen, C.S., Liu, F.H. and Chen, W.R. (2017), "vibration and stability of initially stressed sandwich plates with FGM face sheets in thermal environments", *Steel Compos. Struct.*, **23**(3), 251-261.

Chen, W.Q., Bian, Z.G. and Ding, H.U., (2004), "Three-dimensional vibration analysis of fluid-filled orthotropic FGM cylindrical shells", *Int. J. Mech. Sci.*, **46**(1), 159-171.

Civalek, Ö. (2005), "Geometrically nonlinear dynamic analysis of doubly curved isotropic shells resting on elastic foundation by a combination of HDQ-FD methods", *Int. J. Press Vessel Pip.*, **82**(6), 470-479.

Fantuzzi, N., Tornabene, F., Bacciocchi, M. and Dimitri, R., (2016), "Free vibration analysis of arbitrarily shaped functionally carbon nanotube-reinforced plates", *Composites: Part B*, **115**(1), 384-408.

Fidelus, J.D., Wiesel, E., Gojny, F.H., Schulte K. and Wagner, H.D. (2005), "Thermo-mechanical properties of randomly oriented carbon/epoxy nanocomposites", *Composites: Part A*, **36**(11), 1555-1561.

Gang, S.W., Lam, K.Y. and Reddy, J.N. (1999), "The elastic response of functionally graded cylindrical shells to low-velocity", *Int. J. Impact Eng.*, **22**(4), 397-417.

Ghavamian, A., Rahmandoust, M. and Öchsner, A. (2012), "A numerical evaluation of the influence of defects on the elastic modulus of single and multi-walled carbon nanotubes", *Comput. Mater. Sci.*, **62**, 110-116.

Gojny, F.H., Wichmann, M.H.G., Fiedler, B. and Schulte K. (2005), "Influence of different carbon nanotubes on the mechanical properties of epoxy matrix composites-A comparative study", *Compos. Sci. Technol.*, **65**(15-16), 2300-2313.

Gunawan, H. and Sato, M. (2006), "Free vibration characteristics of cylindrical shells partially buried in elastic foundations", *J. Sound Vib.*, **290**(3-5), 785-793.

Halpin, J.C. and Tsai, S.W. (1969), "Effects of environmental factors on composite materials", AFML-TR-67-423.

Heshmati, M. and Yas, M.H. (2013), "Vibrations of non-uniform functionally graded MWCNTs-polystyrene nanocomposite beams under action of moving load", *Mater. Des.*, **46**, 206-218.

Hong, M. and Lee, U. (2015), "Dynamics of a functionally graded material axial bar, Spectral element modeling and analysis", *Composites: Part B*, **69**, 427-434.

Kamarian, S., Yas, M.H., and Pourasghar, A. (2013), "Free vibration analysis of three-parameter functionally graded material sandwich plates resting on Pasternak foundations", *Sandw. Strut. Mater.*, **15**(3) 292-308.

Kashtalyan, M. and Menshykova, M. (2009), "Three-dimensional elasticity solution for sandwich panels with a functionally graded

core", *Compos. Struct*., **87**(1), 36-43.
Li, Q., Iu, V.P. and Kou, K.P. (2008), "Three-dimensional vibration analysis of functionally graded material sandwich plates", *J. Sound Vib*., **311**(1-2), 498-515.
Loy, C.T., Lam, K.Y. and Reddy, J.N. (1999), "Vibration of functionally graded cylindrical shells", *Int. J. Mech. Sci*., **41**(3), 309-324.
Marin, M. (2010), "A domain of influence theorem for microstretch elastic materials, *Nonlinear Anal. Real World Appl*., **11**(5), 3446-3452.
Marin, M. and Lupu, M. (1998), "On harmonic vibrations in thermoelasticity of micropolar bodies", *J. Vib. Control*, **4**(5), 507-518.
Marin, M. and Marinescu, C. (1998), "Thermoelasticity of initially stressed bodies. Asymptotic equipartition of energies", *Int. J. Eng. Sci*., **36**(1), 73-86.
Martone, A., Faiella, G., Antonucci, V., Giordano, M. and Zarrelli, M. (2011), "The effect of the aspect ratio of carbon nanotubes on their effective reinforcement modulus in an epoxy matrix", *Compos. Sci. Technol*., **71**(8), 1117-1123.
Matsunaga, H. (2008), "Free vibration and stability of functionally graded shallow shells according to a 2-D higher-order deformation theory", *Compos. Struct*., **84**(2), 132-146.
Montazeri, A., Javadpour, J., Khavandi, A., Tcharkhtchi, A. and Mohajeri, A. (2010), "Mechanical properties of multi-walled carbon nanotube/epoxy composites", *Mater. Des*., **31**, 4202-4208.
Moradi-Dastjerdi, R. and Momeni-Khabisi, H. (2016), "Dynamic analysis of functionally graded nanocomposite plates reinforced by wavy carbon nanotube", *Steel Compos. Struct.*, **22**(2), 277-299.
Paliwal, D.N., Kanagasabapathy, H. and Gupta, K.M. (1995), "The large deflection of an orthotropic cylindrical shell on a Pasternak foundation", *Compos. Struct*., **31**, 31-37.
Paliwal, D.N., Pandey, R.K. and Nath, T. (1996), "Free vibration of circular cylindrical shell on Winkler and Pasternak foundation", *Int. J. Press. Vessel Pip*., **69**(1), 79-89.
Park, W.T., Han, S.C., Jung, W.Y. and Lee, W.H. (2016), "Dynamic instability analysis for S-FGM plates embedded in Pasternak elastic medium using the modified couple stress theory", *Steel Compos. Struct*., **22**(6), 1239-1259.
Patel, B.P., Gupta, S.S., Loknath, M.S.B. and Kadu, C.P. (2005), "Free vibration analysis of functionally graded elliptical cylindrical shells using higher-order theory", *Compos. Struct.*, **69**(3), 259-270.
Pelletier Jacob, L. and Vel Senthil, S. (2006), "An exact solution for the steady state thermo elastic response of functionally graded orthotropic cylindrical shells", *Int. J. Solid Struct.*, **43**(5), 1131-1158.
Pradhan, S.C., Loy, C.T., Lam, K.Y., Reddy, J.N. (2000). "Vibration characteristic of functionally graded cylindrical shells under various boundary conditions", *Appl. Acoust*., **61**(1), 119-129.
Pradyumna, S. and Bandyopadhyay, J.N. (2008), "Free vibration analysis of functionally graded panels using higher-order finite-element formulation", *J. Sound Vib*., **318**(1-2), 176-192.
Shakeri, M., Akhlaghi, M. and Hosseini, S.M. (2006), Vibration and radial wave propagation velocity in functionally graded thick hollow cylinder", *J Compos. Struct*., **76**(1), 174-181.
Shu, C. (2000), Differential quadrature and its application in engineering. Springer, Berlin.
Sobhani Aragh, B. and Yas, M.H. (2010), "Static and free vibration analyses of continuously graded fiber-reinforced cylindrical shells using generalized power-law distribution", *Acta Mech*., **215**(1), 155-173.
Sobhani Aragh, B. and Yas, M.H. (2010), "Three dimensional free vibration of functionally graded fiber orientation and volume fraction of cylindrical panels", *Mater. Des*., **31**(9), 4543-4552.
Tahouneh, V. (2014), "Free vibration analysis of bidirectional functionally graded annular plates resting on elastic foundations using differential quadrature method", *Struct. Eng. Mech.*, **52**(4), 663-686.
Tahouneh, V. (2016), "Using an equivalent continuum model for 3D dynamic analysis of nanocomposite plates", *Steel Compos. Struct.*, **20**(3), 623-649.
Tahouneh, V. and Naei, M.H. (2014), "A novel 2-D six-parameter power-law distribution for three-dimensional dynamic analysis of thick multi-directional functionally graded rectangular plates resting on a two-parameter elastic foundation", *Meccanica*, **49**(1), 91-109.
Tornabene, F. (2009), "Free vibration analysis of functionally graded conical cylindrical shell and annular plate structures with a four-parameter power-law distribution", *Comput. Meth. Appl. Mech. Eng*., **198**(37), 2911-2935.
Tornabene, F. and Ceruti, A. (2013), "Mixed static and dynamic optimization of four-parameter functionally graded completely doubly curved and degenerate shells and panels using GDQ method", *Math. Probl. Eng*., 1-33.
Tornabene, F., Fantuzzi, N. and Bacciocchi, M. (2014), "Free vibrations of free-form doubly curved shells made of functionally graded materials using higher-order equivalent single layer theories", *Composites: Part B*, **67**(1), 490-509.
Tornabene, F., Fantuzzi, N. and Bacciocchi, M. (2016b), "Linear static response of nanocomposite plates and shells reinforced by agglomerated carbon nanotubes", *Composites: Part B*, **115**(1), 449-476.
Tornabene, F., Fantuzzi, N., Bacciocchi, M. and Viola, E. (2016a), "Effect of agglomeration on the natural frequencies of functionally graded carbon nanotube-reinforced laminated composite doubly-curved shells", *Composites: Part B*, **89**(1), 187-218.
Viola, E., and Tornabene, F. (2009), "Free vibrations of three-parameter functionally graded parabolic panels of revolution", *Mech. Res. Commun*., **36**(5), 587-594.
Wagner, H.D., Lourie, O. and Feldman, Y. (1997), "Stress-induced fragmentation of multiwall carbon nanotubes in a polymer matrix", *Appl. Phys. Lett.*, **72**(2), 188-190.
Wu, C.P. and Liu, Y.C. (2016), "A state space meshless method for the 3D analysis of FGM axisymmetric circular plates", *Steel Compos. Struct.*, **22**(1), 161-182.
Yang, J. and Shen, S.H. (2003), "Free vibration and parametric resonance of shear deformable functionally graded cylindrical panels", *J. Sound Vib*., **261**(5), 871-893.
Yang, R., Kameda, H. and Takada, S. (1998), "Shell model FEM analysis of buried pipelines under seismic loading", *Bull Disaster Prev Res. Inst*., **38**, 115-146.
Yeh, M.K., Tai, N.H. and Liu, J.H. (2006), "Mechanical behavior of phenolic-based composites reinforced with multi-walled carbon nanotubes", *Carbon*, **44**(1), 1-9.
Zenkour, A.M. (2005a), "A comprehensive analysis of functionally graded sandwich plates. Part 1-deflection and stresses", *Int. J. Solid Struct.*, **42**(1), 5224-5242.
Zenkour, A.M. (2005b), "A comprehensive analysis of functionally graded sandwich plates. Part 1-buckling and free vibration deflection and stresses", *Int. J. Solid Struct.*, **42**(18), 5243-5258.

CC

Appendix

$$F_{1r}=c_{11}\frac{\partial^2}{\partial r^2}+\frac{\partial c_{11}}{\partial r}\frac{\partial}{\partial r}+\frac{\partial c_{12}}{r\partial r}+\frac{c_{66}}{r^2}\frac{\partial^2}{\partial\theta^2}+c_{55}\frac{\partial^2}{\partial z^2}+\frac{c_{11}}{r}\frac{\partial}{\partial r}-\frac{c_{22}}{r^2}$$

$$F_{1\theta}=-\frac{c_{12}}{r^2}\frac{\partial}{\partial\theta}+\frac{c_{12}}{r}\frac{\partial^2}{\partial r\partial\theta}+\frac{\partial c_{12}}{r\partial r}\frac{\partial}{\partial\theta}+\frac{c_{66}}{r}\frac{\partial^2}{\partial\theta\partial r}-\frac{c_{66}}{r^2}\frac{\partial}{\partial\theta}+\frac{c_{12}}{r^2}\frac{\partial}{\partial\theta}-\frac{c_{22}}{r^2}\frac{\partial}{\partial\theta}$$

$$F_{1z}=c_{13}\frac{\partial^2}{\partial r\partial z}+\frac{\partial c_{13}}{\partial r}\frac{\partial}{\partial z}+c_{55}\frac{\partial^2}{\partial z\partial r}+\frac{c_{13}}{r}\frac{\partial}{\partial z}-\frac{c_{23}}{r}\frac{\partial}{\partial z}$$

$$F_{2r}=\frac{c_{66}}{r}\frac{\partial^2}{\partial r\partial\theta}+\frac{\partial c_{66}}{r\partial r}\frac{\partial}{\partial\theta}+\frac{c_{12}}{r}\frac{\partial^2}{\partial r\partial\theta}+\frac{c_{22}}{r^2}\frac{\partial}{\partial\theta}+\frac{c_{66}}{r^2}\frac{\partial}{\partial\theta}$$

$$F_{2\theta}=c_{66}\frac{\partial^2}{\partial r^2}+\frac{\partial c_{66}}{\partial r}\frac{\partial}{\partial r}-\frac{\partial c_{66}}{r\partial r}+\frac{c_{22}}{r^2}\frac{\partial^2}{\partial\theta^2}+c_{44}\frac{\partial^2}{\partial z^2}+\frac{c_{66}}{r}\frac{\partial}{\partial r}-\frac{c_{66}}{r^2}$$

$$F_{2z}=\frac{c_{23}}{r}\frac{\partial^2}{\partial\theta\partial z}+\frac{c_{44}}{r}\frac{\partial^2}{\partial z\partial\theta}$$

$$F_{3r}=c_{55}\frac{\partial^2}{\partial r\partial z}+\frac{\partial c_{55}}{\partial r}\frac{\partial}{\partial z}+c_{13}\frac{\partial^2}{\partial z\partial r}+\frac{c_{23}}{r}\frac{\partial}{\partial z}+\frac{c_{55}}{r}\frac{\partial}{\partial z}$$

$$F_{3\theta}=\frac{c_{44}}{r}\frac{\partial^2}{\partial\theta\partial z}+\frac{c_{23}}{r}\frac{\partial^2}{\partial\theta\partial z}$$

$$F_{3z}=c_{55}\frac{\partial^2}{\partial r^2}+\frac{\partial c_{55}}{\partial r}\frac{\partial}{\partial r}+\frac{c_{44}}{r^2}\frac{\partial^2}{\partial\theta^2}+c_{33}\frac{\partial^2}{\partial z^2}+\frac{c_{55}}{r}\frac{\partial}{\partial r}$$